

Supporting online material

Materials and Methods

Single-walled carbon nanotube (SWNT) devices are fabricated using standard photolithographic techniques (1). Molybdenum electrodes (50 nm thick) are deposited by electron beam evaporation onto a degenerately doped silicon substrate with 100 nm layer of silicon oxide. The Mo electrodes form the split gates above which an additional 100nm Si oxide layer is deposited using plasma enhanced chemical vapor deposition (PECVD). Iron nano-particle catalyst sites are defined and NTs (with diameters of 1-4 nm) are grown by chemical vapor deposition at 700 - 1050 °C. Finally, metallic electrodes (5 nm Cr, 50 nm Au) form the contacts for the NT device. The device channel length is 3-4 micron long from contact to contact with 1 micron of gated region over each of the split gates. Transistor characteristics are measured by sweeping the buried metallic gates (V_1 and V_2) and the global silicon back gate (V_G) at equal voltages, resulting in either p-type or n-type conduction behavior typical of SWNT field effect transistors. Devices showing a substantial “off” region between p-type and n-type conductance are selected for experimentation. Nanotube diameters are measured using a Dimension 3100 atomic force microscope (AFM).

Supporting Text

Split gate devices are placed in an optical scanning microscope setup (figure S1) that combines electronic transport measurements with spatially scanned laser illumination (2, 3). Light sources include a Koheras SuperK Compact broadband supercontinuum

source (light source LS 1) used with a Princeton Instruments monochromator for high resolution spectra, an argon/krypton CW tunable laser (LS 2), and a tunable continuous wave (CW) IR laser (Ando Q4321 1520-1620 nm wavelength) (LS 3). The collimated excitation beam is expanded (beam expander BE) to fill the back aperture of the microscope (MIC) objective, while a CCD camera is used to image and locate the device. A diffraction-limited beam spot is scanned (using a two axis piezo-controlled scanning mirror PSM) over the NT device and the device current is recorded to form a spatial map of photocurrent (figure S2). Photocurrent image resolution is limited by the wavelength of light used, and the beam spot diameter is determined from the full width at half maximum of the observed photocurrent spot. Reflected light from the sample is collected (as a photo voltage V_{REF} in a photo-diode detector PD) and the reflected intensity is monitored to form a simultaneous image of the device. The absolute location of the photo-induced signal is found by comparing the photocurrent map to the reflection image. The devices are mounted in an Oxford HiRes helium optical cryostat (CRYO) that can be cooled to 4 K. Incident laser power is measured at the output of the microscope objective using a calibrated photo-detector. Electrical feed-through allows electronic transport measurements while the device is being illuminated at various temperatures. All measurements are taken in the linear optical power response regime with light polarized (using standard polarization optics P) along the length of the tube to ensure maximum signal with the device configured as a p-i-n junction (1).

Figure S2 shows typical scanning photocurrent images of the SWNT p-n junction. Figure S2 (A) exhibits typical device response for a SWNT device with $V_{SD} = V_G = 0$ V.

Correlating the reflection image (top) to the photocurrent spot (bottom) indicates that the photocurrent occurs over the p-n junction. In figure S2 (B), we show the photocurrent images from which the line cuts of figure 4D were extracted.

As seen in figure S3 and referenced in the main text, we observe device breakdown in the I - V_{SD} characteristics at high reverse bias under illumination that we attribute to standard avalanche multiplication. We plot I - V_{SD} characteristics with the laser fixed on the center of the p-n junction at photon energies below ($E_{PHOTON} < E_{22}$) and above ($E_{PHOTON} > E_{22}$) the threshold for electron-hole pair creation. In addition to multiple electron-hole pair production (region I), we observe the onset to device breakdown at $V_{SD} \sim -3$ V (region II). Since it occurs for both illuminated characteristics, we attribute this to the standard impact ionization process:

$$e_1 + K_e \rightarrow e_1 + n(e_1 + h_1).$$

In SWNTs, large-energy ($\hbar \omega \sim 0.18$ eV) optic phonon emission is believed to be the dominant energy loss mechanism at high injection currents (4-6) and occurs with a mean free path $l_{OP} \sim 30$ nm. In order for a charge carrier to undergo impact ionization while competing with optic phonon emission, the device must reach the breakdown voltage (1): $V_{br} > (\hbar \omega / e l_{OP}) L \sim 6$ V. This simple estimate is roughly consistent with the breakdown behavior in the I - V_{SD} characteristics of figure S2.

Supporting figure legends

Figure S1 Schematic of optoelectronic setup for measuring photocurrent in the SWNT p-n junction. Components are labeled in text, except for common elements: mirrors (M) and beam-splitters (BS). **Inset:** CCD camera capture of device structure with various electrodes labeled. V_1 and V_2 are the split gates and V_G is the global back gate. Electrodes labeled V_{SD} and I are the gold electrodes contacting the SWNT. Scale bar 20 microns.

Figure S2 Scanning photocurrent microscopy of the SWNT p-n junction.

(A) top, typical reflection image of split gate device. Red areas are regions of high reflection (due to the gold electrode) and blue/black are areas of low reflection (silicon/SiO₂ substrate). **bottom,** correlated photocurrent map collected simultaneously to reflection image. Photocurrent spot occurs at the p-n junction. Scale bar 5 microns. **(B)** Reflection and corresponding photocurrent images at low temperatures in forward bias as in figure 4C of main text. Scale bar 1 micron.

Figure S3 I - V_{SD} characteristics of the SWNT p-n junction at high reverse

bias. Device characteristics at various photon energies (labeled) for the device (and same experimental conditions) of figure 4F in main text. Laser fixed at the center of the device. Region I labels the region in which multiple electron-hole

pair creation occurs. Region II labels the region of conventional high bias avalanche multiplication.

Supporting figures

Figure S1

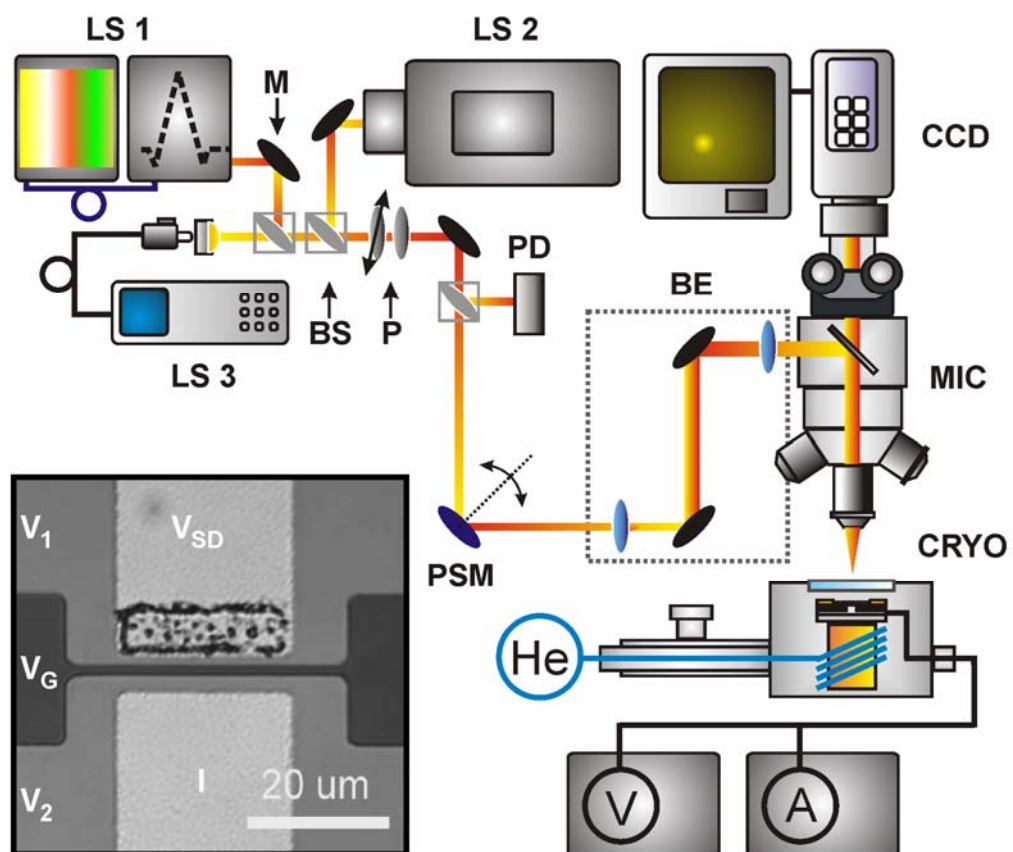


Figure S2

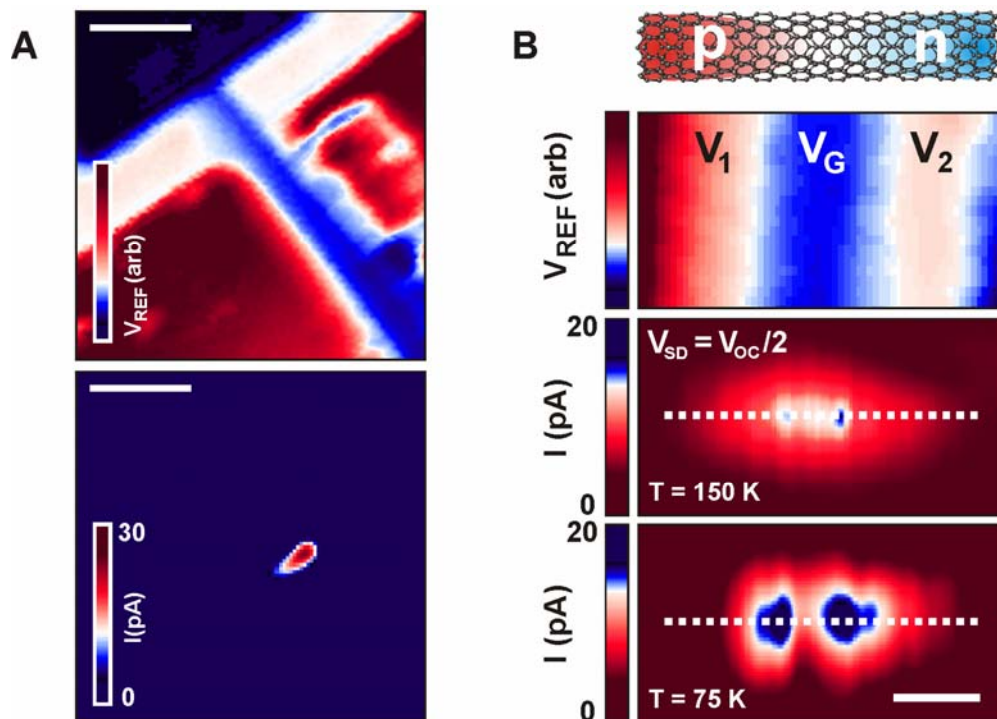
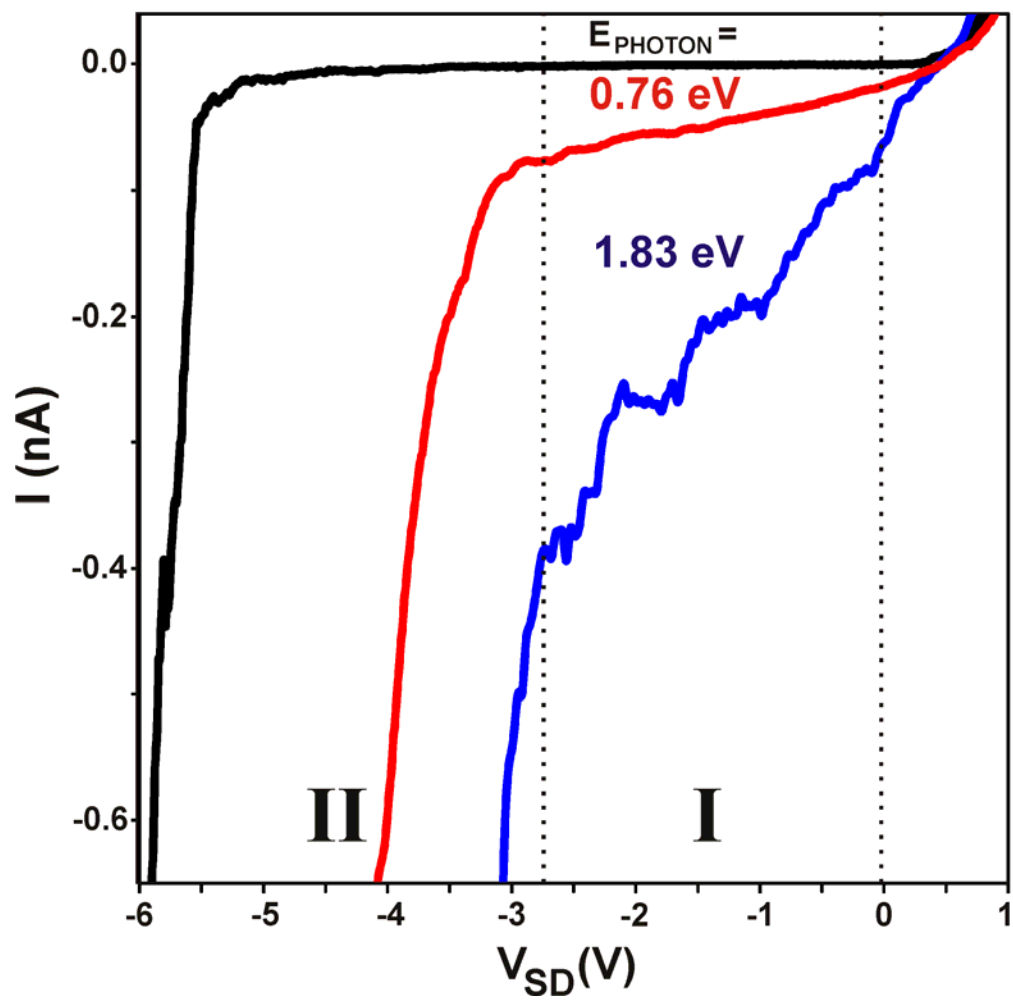


Figure S3



Supporting references and notes

1. Bosnick, K., Gabor, N.M., McEuen, P.L. *Applied Physics Letters* **89**, 163121 (2006).
2. Balasubramanian, K. et al. *Applied Physics Letters* **84** (13), 2400-2402 (2004).
3. Ahn, Y., Dunning, J., Park, J. *Nano Letters* **5**, 1367 (2005).
4. Park, J. Y., et al. *Nano Letters* **4**, 517 (2004).
5. Pop, E. et al. *Physical Review Letters*, **95**, 155505-1-4 (2005).
6. Yao, Z., Kane, C. L., Dekker, C. *Physical Review Letters*, **84**, 2941-2944 (2000).